Green Chemistry

PAPER

View Article Online
View Journal | View Issue

Cite this: *Green Chem.*, 2020, **22**, 5115

Cellulose nanocrystals (CNCs) as hard templates for preparing mesoporous zeolite Y assemblies with high catalytic activity†

Samer Abdulridha,[a] Jiuxing Jiang,[b] Shaojun Xu,[a] Zhaoxia Zhou,[c] He Liang,[d] Boyang Mao,[e] Yangtao Zhou,[f] Arthur A. Garforth,[a] Yilai Jiao*[a,f] and Xiaolei Fan*[a]

Received 26th March 2020,
Accepted 25th June 2020

DOI: 10.1039/d0gc01070g

rsc.li/greenchem

Faujasite (FAU) Y zeolite assemblies with high mesoporosity (S_{ext} = 347 m^2 g^{-1} and V_{meso} = 0.52 cm^3 g^{-1}) were synthesised using sustainable and economic cellulose nanocrystals (CNCs) *via* a template-directed synthesis method, *i.e.* CNCs-Y. In comparison with the control zeolite catalysts of the conventional microporous Y and carbon nanotube templated Y (CNTs-Y) zeolites, the resulting CNCs-Y demonstrated superior performance in catalytic dealkylation with excellent activity and longevity, as well as the anti-coking ability thanks to the exceptional mesoporous features of CNCs-Y zeolites. Thereby, the method and relevant CNCs-Y mesoporous zeolites based on the sustainable CNCs presented here have significant implications for being developed further for improving the sustainability of relevant catalytic processes such as fluid catalytic cracking (FCC).

Introduction

Synthetic zeolites are commercially important materials, primarily used as detergent builders, catalysts, and absorbents in a wide range of industries. Zeolite-based catalysts are particularly important to the petrochemical conversion processes,[1,2] represented by fluid catalytic cracking (FCC), which uses >95% of synthetic zeolites in the catalysis sector.[1] Faujasite (FAU) Y zeolites, especially ultra-stable Y, are the key active components in zeolite-based FCC catalysts. Y zeolite is crystalline, microporous (pore width = 0.74 nm) and rigid, offering good mechanical and hydrothermal stability under the severe conditions used in FCC processes (>500 °C).[3,4] Diffusion limitation imposed by intrinsic micropores of zeolites is one of the major causes of low activity and/or deactivation in zeolite catalysis,[5] especially for reactions involving molecules larger than 1 nm.[6,7] Therefore, enormous effort has been spent on overcoming the diffusion limitation and enhancing the accessibility of the active surface within the framework zeolites, leading to the development of the state-of-the-art zeolitic materials such as nanozeolites,[8–10] zeolitised mesoporous materials, and zeolites with mesoporosity (or the so-called mesoporous zeolites).[7,11] Among these, it is a widely held view that zeolites with mesoporosity are practical for further industrial exploitation. Mesoporosity can be created in zeolites *via* either the 'bottom-up' (*i.e.* templating methods) or 'top-down' (*i.e.* post-synthetic treatments) methods,[2,7,12,13] offering practical yet effective solutions to realise the faster molecular transport within the mesoporous zeolites and the greater catalytic activity compared to the conventional microporous zeolites. However, the templating methods are generally less energy intensive than the post-synthesis methods, in which prolonged post-synthesis hydrothermal treatments such as steaming are necessary.[14,15] The use of sacrificial hard templates for preparing mesoporous zeolites is facile and flexible. Specifically, in the hard-templating method, (i) the significant revision of the synthesis protocol of zeolites is usually not needed and (ii) the regulation of the Si/Al ratio (*i.e.* acidity) can be achieved independently from the creation of mesoporosity. Carbon nanostructures such as nanotubes and nanofibers are the most researched hard templates to create various structured zeolites

[a]*Department of Chemical Engineering and Analytical Science, School of Engineering, The University of Manchester, Manchester, M13 9PL, UK. E-mail: xiaolei.fan@manchester.ac.uk*
[b]*MOE Key Laboratory of Bioinorganic and Synthetic Chemistry, Environment and Energy Chemistry, School of Chemistry, Sun Yat-Sen University, Guangzhou 510275, People's Republic of China*
[c]*Loughborough Materials Characterisation Centre, Loughborough University, Loughborough, Leicestershire, LE11 3TU, UK*
[d]*Department of Eye and Vision Science, Institute of Life Course and Medical Sciences, University of Liverpool, 6 West Derby Street, Liverpool, L7 8TX, UK*
[e]*Department of Engineering, University of Cambridge, JJ Thomson Avenue, Cambridge CB3 0FA, UK*
[f]*Shenyang National Laboratory for Materials Science, Institute of Metal Research, Chinese Academy of Sciences, 72 Wenhua Road, Shenyang 110016, People's Republic of China. E-mail: yljiao@imr.ac.cn*

†Electronic supplementary information (ESI) available. See DOI: 10.1039/d0gc01070g

with mesoporosity (2–50 nm, mainly MFI types). However, compatibility issues (where surface treatments using strong mineral acids are usually required), as well as the high costs of these carbon materials (>$1500 per kg),[2,16] make the method using carbon nanostructures unsustainable, especially from an industrial perspective.[2] In this respect, there are always interests to find sustainable hard templates to progress the 'bottom-up' approach such as N-doped carbonaceous monoliths[17] and starch-derived bread.[18]

With the emergence of cost-effective commercial sources of cellulose nanocrystals (CNCs, <$50 per kg), as renewable and sustainable materials, have been shown to provide considerable value in many applications such as nanocomposites.[19,20] Rod-shaped CNCs (average diameter of 5–20 nm; average length of 100–500 nm (ref. 20)) have an inherently high surface area (theoretical value of 550 $m^2\ g^{-1}$) with abundant surface groups (*e.g.* hydroxyl groups), making them ideal as templates in preparing composite materials, which is exemplified by the work on CNCs-templated mesoporous amorphous silicates.[21–24] Unlike the conventional carbon materials, CNCs are intrinsically compatible with zeolite synthesis protocols due to their reactive surfaces and hydrophilicity as a result of the hydroxyl groups on their crystalline facets. Previous research showed that, in the process of zeolite crystallisation, cellulose in the vegetal fibres is the reactive component, rather than lignin and pectin, which interacts with the aluminosilicate species, and hence promotes the formation of zeolite nuclei.[25,26] Specifically, the hydroxyl (–OH) groups in cellulose were believed to be the favourable sites for zeolite crystallisation.[25–27] Recently, Zhao *et al.*[28] have shown the first CNCs-templated synthesis of MFI ZSM-5, delivering with surprisingly high mesopore volumes ($V_{meso} : V_{total} = \sim 1$) and good activity (as nickel-supported catalysts) for the catalytic conversion of microcrystalline cellulose to hexitols (*ca.* 60% yield).[28] Unlike MFI-type zeolites, the 'bottom-up' synthesis of FAU using hard templates[29] is challenging because (i) the structure-directing agents are usually not used and (ii) favourable interactions between the hard templates and the silicate or aluminosilicate species are needed. To date, the majority of successful cases of synthesising Y-type mesoporous zeolitic materials are based on soft templates such as mesoscale cationic surfactants.[30,31]

In this work, we present the synthesis of Y zeolite assemblies with high intercrystal mesoporosity using sustainable commercial CNCs as the hard template. The properties of CNCs-templated Y zeolite (*i.e.* CNCs-Y) such as mesoporous and acidic features are compared with those of the control zeolites of conventional Y zeolite and carbon nanotube (CNT) templated Y zeolite (*i.e.* CNTs-Y) using various characterisation techniques, showing that CNCs-Y possesses well-developed mesoporosity and abundant external surfaces. In addition, comparative catalytic cracking (of 1,3,5-triisopropylbenzene, TiPBz) assessment of the Y zeolites under investigation is carried out, which shows the comparatively excellent catalytic and anti-deactivation performance of CNCs-Y zeolite.

Materials and methods

Chemicals and materials

Chemicals used in the synthesis of Y zeolites included sodium aluminate (Al_2O_3, 55%; Na_2O, 45%; Sigma-Aldrich), Ludox® (AS-40, 40 wt% suspension in H_2O, Sigma-Aldrich), sodium hydroxide (NaOH, 99%, Sigma-Aldrich), ammonium nitrate (NH_4NO_3, ACS reagent ≥98%, Sigma-Aldrich), multiwalled carbon nanotubes (≥98% carbon basis, Sigma-Aldrich), nanocellulose (99%, CelluForce Inc., Canada), and sodium hypochlorite (NaOCl, 99%, Sigma-Aldrich).

Chemicals used in GC calibration and catalytic tests were benzene (C_6H_6, ≥99.8%, Sigma-Aldrich), toluene ($C_6H_5CH_3$, ≥99.5%, Sigma-Aldrich), *para*-xylene ($C_6H_4(CH_3)_2$, ≥99.5% GC, Sigma-Aldrich), *ortho*-xylene ($C_6H_4(CH_3)_2$, ≥99.5% GC, Sigma-Aldrich), *meta*-xylene ($C_6H_4(CH_3)_2$, ≥99.5% GC, Sigma-Aldrich), cumene (C_9H_{12}, 99%, Alfa Aesar), 1,2,3-trimethylbenzene ($C_6H_3(CH_3)_3$, ≥99.5%, neat, GC, Sigma-Aldrich), 1,2,4-trimethylbenzene ($C_6H_3(CH_3)_3$, 98%, Sigma-Aldrich), 1,3-diisopropylbenzene ($C_{12}H_{18}$, 96%, Sigma-Aldrich), 1,4-diisopropylbenzene ($C_{12}H_{18}$, 99%, Alfa Aesar), and 1,3,5-triisopropylbenzene ($C_{15}H_{24}$, 95%, Alfa Aesar). All chemicals were used as received without further purification.

Synthesis of zeolites

A secondary growth method was used to synthesise the conventional Y zeolite. To prepare the colloidal seed with a composition of 10.67 $Na_2O : Al_2O_3 : 10\ SiO_2 : 180\ H_2O$, sodium aluminate (1 g) and sodium hydroxide (4.02 g) were firstly dissolved in distilled water (11.7 ml), and the mixture was stirred until the solution became clear. Ludox solution (8.01 g) was then added dropwise to the mixture under stirring (over 40 min). The colloidal solution was aged statically at room temperature (RT) for 24 h to form the seeds. The synthesis gel was prepared by dissolving 1 g of sodium aluminate and 1.27 g of sodium hydroxide in 12.33 ml of distilled water under stirring for at least 10 min. Afterwards, 8.01 g of Ludox solution was added to the prepared solution, and the mixture was stirred vigorously for 30 min to obtain a composition of 4.30 $Na_2O : 1\ Al_2O_3 : 10\ SiO_2 : 180\ H_2O$. In the secondary growth synthesis, 1.25 g of the colloidal seed gel was added to the synthesis gel (the mass ratio of the seeds to the synthesis gel was 5.5%) under vigorous stirring for 30 min. Then, the mixture (with a composition of 4.62 $Na_2O : 1\ Al_2O_3 : 10\ SiO_2 : 180\ H_2O$) was transferred into an autoclave reactor (50 mL with a PTFE liner, the percentage fill of the mixture in the liner was ~40%) for hydrothermal synthesis at 100 °C for 48 h.

The method was modified to prepare the templated Y zeolites (*i.e.* CNTs-Y and CNCs-Y) using hard templates of multiwalled carbon nanotubes (CNTs, which were oxidised using sodium hypochlorite to reduce the hydrophobicity, see ESI, Fig. S1–S2†) and CNCs (used as received without any further treatment). Hard templates (0.235 g) were added during the preparation of the colloidal seed (after the addition of sodium aluminate and sodium hydroxide) and aged with the seeds for 24 h before the synthesis of templated zeolites. In order to

homogenise the dispersion of hard templates in the colloidal seeds, the mixture was sonicated for 15 min followed by mixing for 20 min before any further use. The template–seeds mixture was then aged (at RT for 24 h) and added (1.3 g) into the synthesis gel for crystallisation under the same conditions. The as-prepared zeolites (with the mass yield of the synthesis in the range of 2.3–2.7 g) from the templating methods were calcined in air at 600 °C for 15 h to remove the hard templates. The resulting zeolites were labelled as *x*-Y, where *x* refers to the hard templates of CNCs or CNTs.

Characterisation of materials

Powder X-ray diffraction (PXRD) patterns of materials were obtained using a Philips X'Pert X-ray diffractometer under the conditions of CuKα_1 radiation, λ = 1.5406 Å, 40 kV, 40 mA, 5° < 2θ < 65°, and 0.0167° step size. Nitrogen (N_2) adsorption–desorption analysis was performed at −196 °C using a Micromeritics 3Flex surface Characterisation Analyser. Prior to N_2 sorption measurements, the sample (~100 mg) was degassed at 350 °C under vacuum overnight. The specific surface areas of the catalysts were determined based on the Brunauer–Emmett–Teller (BET) method. Pore size analysis was performed using the Barrett–Joyner–Halenda (BJH) method with adsorption branch isotherms. Scanning electron microscopy (SEM) and energy dispersive X-ray diffraction (EDX) were performed with a FEI Quanta 250 FEG-SEM instrument using a work distance of 8–10 mm and an accelerating voltage of 15 kV. All samples were dispersed in acetone and dropped onto SEM studs, followed by gold deposition using an Emitech K550X sputter coater under vacuum (1×10^{-4} mbar). Transmission electron microscopy (TEM) micrographs were obtained using a FEI Tecnai G2 F20 electron microscope operated at 200 kV. X-ray fluorescence (XRF) spectroscopy was performed using a PANalytical minipal4 (PANalytical EDXRD) spectrometer operated at 30 kV and 1 mA. Thermogravimetric analysis (TGA) and differential thermal analysis (DTA) were performed using a TG analyser (Beijing Boyuan Science and Technology Development Co., Ltd) at a heating rate of 5 °C min^{-1} from 20 to 600 °C in air (100 mL min^{-1}). A mass spectrometer (MS, Hiden DSMS analyser, Hiden Analytical) was also coupled to the TGA for gas analysis in the experiment of studying the thermal decomposition behaviour of the templated zeolites (at a heating rate of 5 °C min^{-1} from 20 to 600 °C in air at 100 mL min^{-1}). Ammonia temperature programmed desorption (NH_3-TPD) analysis for determining the acid strength and the concentration of acidic sites on the zeolites was performed using a Micromeritics AutoChem II 2920 chemisorption analyser (100 mg sample, 10 °C min^{-1}, He flow rate = 30 cm^3 STP min^{-1}). Fourier transform infrared transmission spectroscopy (FT-IR) was performed in a Bruker Vertex 70 spectrometer with red-light emission from a helium–neon laser, and a wide range MIR-FIR beam splitter and a detector. The spectra were obtained at ambient temperature with 56 scans at 4 cm^{-1} resolution in the wavelength range of 400–1200 cm^{-1}.

Catalysis

Before catalysis, all zeolites were converted to their H-forms *via* ion exchange through three consecutive treatments using 0.1 M aqueous NH_4NO_3 solution (1 g zeolite in 100 mL of solution at 25 °C for 8 h per treatment). The ion-exchanged zeolites were then washed using deionised water and calcined in static air at 450 °C for 5 h at a heating rate of 5 °C min^{-1}. Catalytic cracking of 1,3,5-triisopropylbenzene (TiPBz) over Y zeolites (250 mesh pellets) was performed at 325 °C under atmospheric pressure using a pulse method.[32–35] In a catalytic experiment, 20 mg of zeolite catalysts was packed in a borosilicate glass-tube liner (internal diameter, i.d. = 4 mm; outer diameter, o.d. = 6.3 mm; length = 72 mm; Restek) between two glass wool beds (deactivated glass wool from Restek, Fig. S3†). Then, the reactor tube was inserted into a gas chromatograph (GC) injector and heated to 325 °C (from 50 °C to 325 °C within 2 h and isothermal at 325 °C, 1 h) before injections. Manual injection of 0.2 μL of TiPBz was performed using an Agilent SGE syringe (Trajan, 0.5BNR-5BV/0.63) with helium (He) as the carrier gas (Table S1†). Reactants/products from the cracking reaction were analysed inline using a Varian 3400 GC equipped with a flame ionisation detector (FID). Details of the GC method used are presented in Table S1 and Fig. S4.†

Results and discussion

The crystallisation of FAU Y zeolite is favoured by the presence of seeds,[36] as proved by the systematic development of the secondary growth method for synthesising zeolite Y (ESI, Fig. S5 and S6†). This method was then adopted by adding hard templates of CNCs (commercial CNCs by CelluForce) and CNTs (as the control) during the preparation of the colloidal seeds for preparing Y zeolites with mesoporosity. After the synthesis, all materials were calcined in air at 600 °C before characterisation. Specifically, for CNTs-Y and CNCs-Y, calcination helped to remove the hard templates from the resulting zeolites, as evidenced by TGA-MS (Fig. S7–S8†), which shows the evaluation of MS signals of m/z = 28 and 44, corresponding to CO ad CO_2, respectively.

CNCs possess abundant surface groups, especially surface –OH (Fig. S2†), which are beneficial to the compatibility between CNCs and seed gel, and hence the subsequent secondary growth synthesis. Previous research has shown that hydroxyl ions in the alumosilicate gel could destroy the hydrogen bonds between the cellulose chains, and hence facilitating the nucleation process.[26] SEM (Fig. 1) and EDX (Fig. S9†) analyses showed that the CNC-directed synthesis promoted the seed surround around CNCs (SEM of CNCs is shown in Fig. S10†). Followed by crystallisation under hydrothermal conditions, nanosized Y (*i.e.* CNCs-Y, Fig. 2a and b) with intercrystal mesopores (Fig. 2c and d) were formed, which was confirmed by the morphological characterisation using SEM and TEM. In addition, SEM micrographs (Fig. 2a and b) show that CNCs promoted spherical Y assemblies of about 1–3 microns with individual crystal sizes of 200–500 nm. TEM images

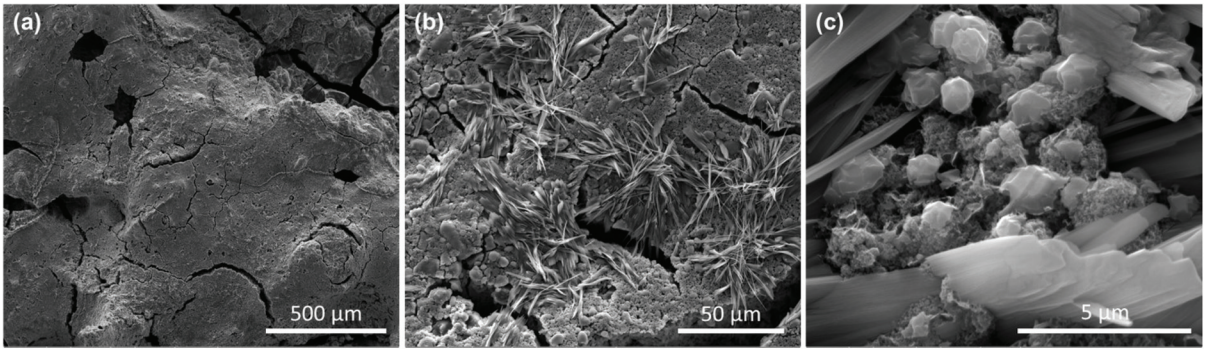

Fig. 1 (a)–(c) SEM micrographs of the as-prepared CNCs-Y seed gel composite.

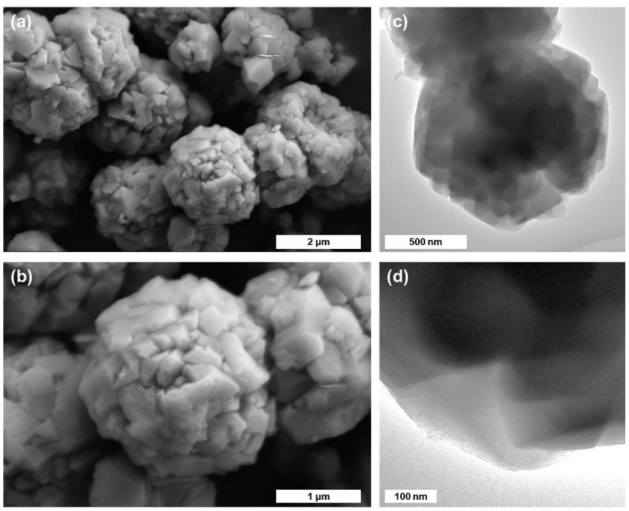

Fig. 2 (a) and (b) SEM micrographs and (c) and (d) TEM images of CNCs-Y zeolites.

(Fig. 2c and d) show the presence of (i) dense and lighter features of Y assemblies and (ii) dense and uniform crystalline region in the individual crystal in CNCs-Y, suggesting the intercrystal mesoporosity in CNCs-Y. Such mesoporous features may endow CNCs-Y with the substantial specific external surface area and mesopore volume. Accordingly, the modification of the seed sol with CNCs played a dominating role in promoting the formation of Y nanocrystal aggregates with intercrystal mesopores. Conversely, CNTs-Y showed the morphology of assemblies, but with the average diameter of <1 µm (Fig. S11†).

XRD analysis (Fig. 3a) shows that CNCs-Y and CNTs-Y have the characteristic diffraction pattern of the FAU-type structure of Y. Fig. 3b presents the comparison of N_2 adsorption–desorption isotherms of materials, in which CNCs-Y and CNTs-Y show the physisorption hysteresis of type H2,[37] suggesting the presence of mesoporosity in these materials. Relevant textural properties of the zeolite under investigation are shown in Table 1. In comparison with CNTs, CNCs are more capable of promoting the formation of mesopores during the template-directed synthesis of Y. Pore size distributions using the BJH method (Fig. 3c) show the bimodal distribution of well-developed mesopores in CNCs-Y (2–22 nm), while mesopores in CNTs-Y centre at around 20 nm. Both the pristine Y zeolite and the reference CNTs-Y possess significantly lesser mesopore volumes (V_{meso} = 0.03 and 0.09 $cm^3\ g^{-1}$ for Y and CNTs-Y,

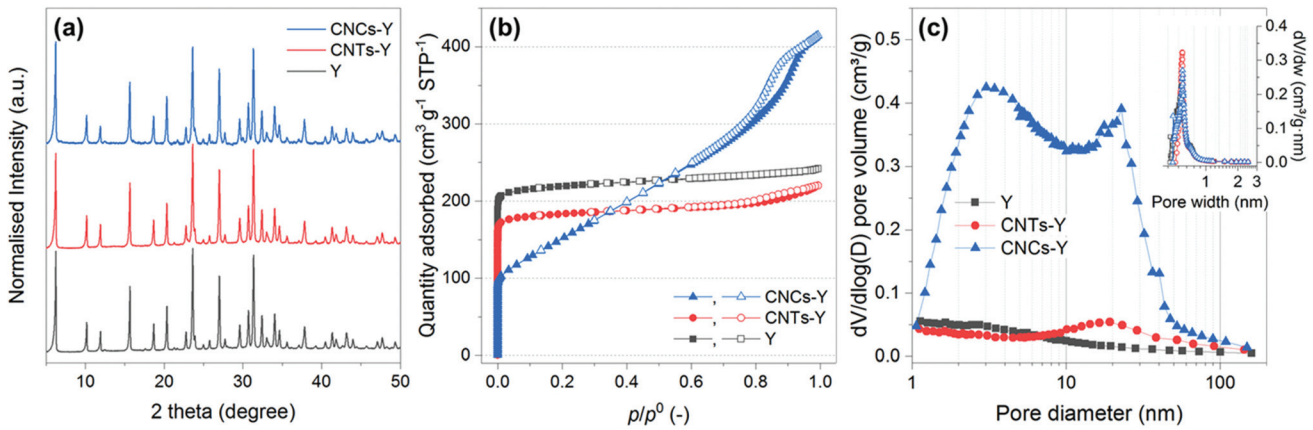

Fig. 3 The comparison of (a) XRD patterns, (b) N_2 adsorption–desorption isotherms and (c) BJH pore size distributions (based on the adsorption branch of isotherms, inset: Horváth–Kawazoe (H–K) pore size distributions) for the pristine Y, CNTS-Y and CNCs-Y zeolites prepared by the secondary growth method (48 h synthesis).

Table 1 Textural properties and elemental data analysis of Y, CNTs-Y and CNCs-Y zeolites

	Nitrogen physisorption data						
Sample	S_{BET} [$m^2\ g^{-1}$]	V_{total} [a] [$cm^3\ g^{-1}$]	V_{micro} [b] [$cm^3\ g^{-1}$]	V_{meso} [c] [$cm^3\ g^{-1}$]	S_{micro} [b] [$m^2\ g^{-1}$]	$S_{ext.}$ [b] [$m^2\ g^{-1}$]	Si/Al[d] [–]
Y	716	0.35	0.32	0.03	681	35	2.6
CNCs-Y	522	0.64	0.12	0.52	175	347	2.9
CNTs-Y	683	0.34	0.25	0.09	614	69	2.8

[a] Single point adsorption total pore volume at $p/p^0 = 0.99$; [b] *t*-Plot method; [c] $V_{total} - V_{micro}$; [d] By XRF.

respectively) than CNCs-Y (0.52 $cm^3\ g^{-1}$). Apparently, CNTs are not effective as hard templates to facilitate the formation of mesoporosity in the synthesis protocol used in this work. It is also worth noting that the microporous feature of CNCs-Y is comparatively less significant than that of the pristine Y and CNTs-Y, as shown in Table 1, which could be attributed to the presence of the non-microporous amorphous aluminosilicate matrix in the resulting CNCs-Y,[38] as confirmed by the ^{29}Si solid-state nuclear magnetic resonance spectroscopy (Fig. S12†). Findings from N_2 adsorption–desorption analysis confirm those from SEM/TEM. Since the synthesis protocol was in principle the same, apart from the hard templates used in the templating methods, the relevant CNCs-Y and CNTs-Y zeolites showed comparable silicon-to-aluminum (Si/Al) molar ratios, as confirmed by XRF (Table 1). This work shows the potential of CNCs as hard templates for making Y zeolites with mesoporous features, which should be further explored, such as the seed formation and crystallisation in the presence of CNCs and effect of the properties of CNCs (such as size and shape on the synthesis) on the physical/chemical properties of the resulting zeolites.

As the utmost important additive in FCC catalysts, Y zeolites with mesoporosity[39] have been proved to be extremely beneficial for refineries, even at the industrial scale (*e.g.* the mesoporous Y prepared by the surfactant-templated post-synthetic modification[40]). To demonstrate the application potential of the Y assemblies templated by CNCs for heavy distillate conversion, the catalytic cracking performance of CNCs-Y with reference to the pristine Y and CNTs-Y was assessed using a pulse method.[33,35,41,42] 1,3,5-Triisopropylbenzene (TiPBz), a typical compound to study the dealkylation reactions over FCC catalysts,[41–45] was used as the bulky model molecule. TiPBz has a critical diameter of 0.95 nm,[45] being larger than the intrinsic pore width of FAU Y (*i.e.* 0.74 nm), suggests that the external surface area ($S_{ext.}$) of the zeolite catalysts will play a significant role in promoting the cleavage of alkyl groups.

The catalytic results of the cracking reactions (Fig. 4a and Fig. S13–S16†) show the superior performance of CNCs-Y (regarding the absolute conversion of TiPBz) over the pristine Y and CNTS-Y. In details, the pristine Y promoted the conversion of TiPBz at 71% at the first pulse (or injection), then rapidly deactivated to only 9% after nine injections, suggesting rapid coke disposition on the external surface of pristine Y zeolite crystals. In trials of using the control CNTs-Y catalyst,

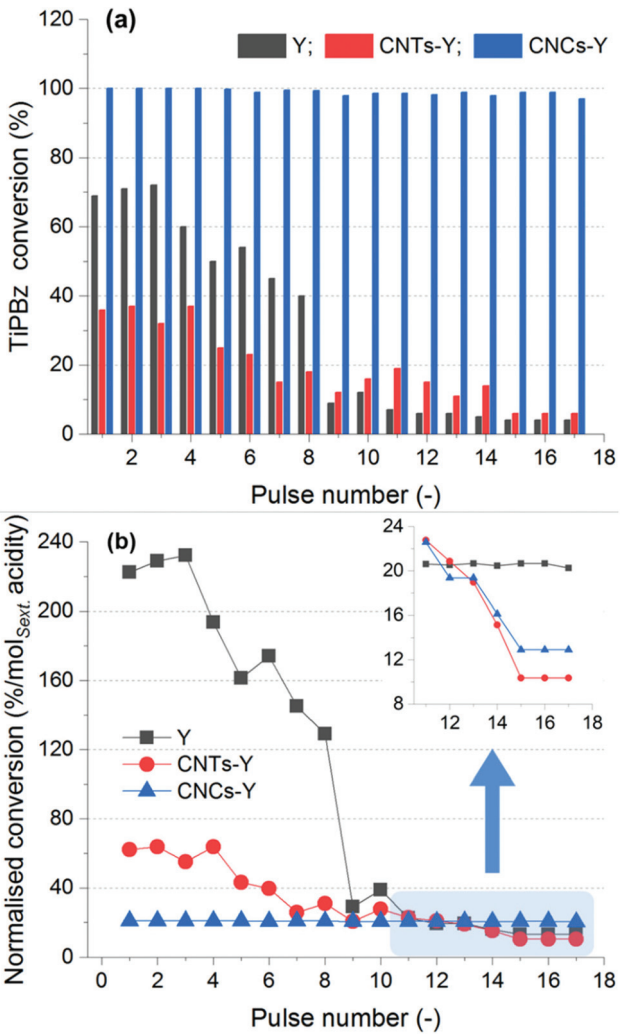

Fig. 4 (a) Conversion and (b) normalised conversion of TiPBz over Y, CNCs-Y and CNTs-Y zeolites as a function of pulse number.

over the course of the pulse experiment, CNTs-Y lost its activity (represented by TiPBz conversion) gradually from 37% to 6%. Conversely, CNCs-Y showed a remarkable catalytic activity with >97% TiPBz conversions in the comparative catalytic assessment. Generally, strong acidic sites in FAU Y (provided by the alumina tetrahedra) and the amorphous aluminosilicate matrix are believed to be responsible for the

Table 2 Acidic properties of Y, CNTs-Y, and CNCs-Y zeolites (after ion exchange)

Sample	Temperature at maximum [°C]		Weak acidity [mmol g^{-1}]	Strong acidity [mmol g^{-1}]
	First peak	Second peak		
Y	201	309	0.297	0.315
CNTs-Y	214	318	0.553	0.289
CNCs-Y	201	264	0.219	0.360

dealkylation.[38,46,47] However, the accessibility of the acidic sites depends on the porous structures of the zeolite framework, making the coupled effect on the catalytic performance challenging to be fully understood. By performing NH_3-TPD analysis, the concentration and strength of surface acidic sites of the three zeolite catalysts were revealed, as shown in Table 2 and Fig. S17.† Specifically, the strong acidity of the three zeolites is comparable (*i.e.* the concentration of strong acidic sites, as determined by NH_3-TPD for NH_3 desorption at 300 ± 30 °C). Herein, we assume that (i) the strong acidity dominates zeolite catalysis and (ii) the distribution of acidic sites throughout the pore surface (including both micropore and mesopore surfaces) is homogeneous and uniform. Accordingly, the absolute conversion of TiPBz can be normalised using the external surface strong acidity ($S_{ext.}$ acidity in mmol g^{-1}, as defined by eqn(1)) to estimate the effectiveness of the catalysts in the model reaction, approximately, as shown in Fig. 4b.

$$S_{ext}\ \text{acidity} = \text{Strong acidity} \times (S_{ext}/S_{BET}) \quad (1)$$

Interestingly, at initial injections (pulse number <9), the comparison of normalised conversions of catalysts shows that the pristine Y and CNTS-Y are more effective than CNCs-Y. For example, the normalised conversion of Y was ten times higher than that of CNCs-Y at the initial three injections. This result suggests that the external surface areas of Y and CNTS-Y are mainly from the external crystal surface, rather than from the intercrystal mesopores. They were readily accessible, but deactivated fast due to coke deposition on the external surface of Y zeolite crystals, blocking all the acidic sites within the zeolitic framework. However, for CNCs-Y, the presence of intercrystal mesoporosity sustained the steady and healthy molecular diffusion and reaction, leading to the measured high absolute conversion and steady normalised conversion during the entire catalytic test. The excellent anti-deactivation property of CNCs-Y is also reflected by TGA of the used catalysts (Fig. 5). By subtracting the weight loss of samples at 600 °C from that at 150 °C, CNCs-Y shows the lowest weight loss of about 4.9%, while ~6.7% was measured for the pristine Y and CNTs-Y, evidencing the reduced coke formation due to the mesoporosity. The detailed analysis of the selectivity is presented in Fig. S15,† showing that cumene and propylene are the main products from the model cracking reaction. Among the three catalysts, CNCs-Y gives the highest total selectivity to propylene and cumene (89% ± 3%) compared to CNTs-Y (70% ± 9%) and Y (84% ± 0.8%), demonstrating its good ability in dealkylation. More importantly, the comparison of product yields (Fig. S16†) shows that CNCs-Y can be advantageous for practical FCC applications due to their well-developed intercrystal mesoporosity.

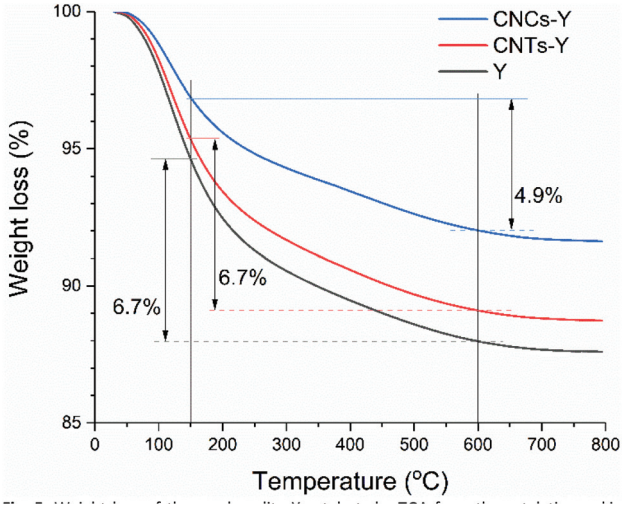

Fig. 5 Weight loss of the used zeolite Y catalysts by TGA from the catalytic cracking experiments.

Conclusion

Mesoporous zeolites are important materials for practical catalysis, and the sustainable synthesis of mesoporous zeolites can be beneficial for the down-stream conversion processes regarding the reduction of carbon footprints and improvement of process sustainability. Here, we demonstrated that the readily available and renewable cellulose nanocrystals (CNCs) can be used as cost-effective and sustainable templates to prepare Y zeolites with a significantly high intercrystal mesoporosity with S_{ext} = 347 m^2 g^{-1} and V_{meso} = 0.52 cm^3 g^{-1}, being one of the highest among the state-of-the-art relevant materials prepared by the 'bottom-up' methods (Table S2†). The well-developed mesoporosity and abundant external surfaces of CNCs-Y, which make the active catalytic sites accessible to the probe molecules, were translated into the comparatively excellent catalytic and anti-deactivation performance in cracking of TiPBz, surpassing the control catalysts under investigation, *i.e.* the conventional microporous Y and CNTs-Y. This work demonstrated the potential of using sustainable CNCs to replace the conventional expensive and/or toxic soft/hard templates for making mesoporous zeolites, being significant to the sustainable development of relevant conversion processes. More importantly, the presented method (of employing CNCs for the synthesis of a mesoporous Y zeolite) may stimulate new ideas and research avenues of using biomass-derived sustainable nanocellulose (*e.g.* CNCs, cellulose nanofibrils, and cellulose nanowhiskers) in zeolite chemistry and catalysis.

Conflicts of interest

There are no conflicts to declare.

Acknowledgements

This project has received funding from the European Union's Horizon 2020 research and innovation programme under grant agreement No. 872102. SA was supported by The Higher Committee for Education Development in Iraq *via* a postgraduate research scholarship. YJ thanks the financial support from the Liaoning Provincial Natural Science Foundation of China (20180510012) and the China Scholarship Council (CSC) for his academic visiting fellowship in the UK (file no. 201604910181).

References

1 W. Vermeiren and J.-P. Gilson, *Top. Catal.*, 2009, **52**, 1131.
2 R. Chal, C. Gérardin, M. Bulut and S. van Donk, *ChemCatChem*, 2011, **3**, 67.
3 J. Čejka, G. Centi, J. Perez-Pariente and W. J. Roth, *Catal. Today*, 2012, **179**, 2.
4 V. Valtchev, G. Majano, S. Mintova and J. Perez-Ramirez, *Chem. Soc. Rev.*, 2013, **42**, 263.
5 P. Selvam, J. Sauer, B. Garrett, C. Campbell, R. van Santen, P. Davies, A. L. Miller, M. Bowker, G. Hutchings, D. Wotton, H.-J. Freund, M. Howard, M. Feaviour, R. Burch, A. M. R. Galletti, E. Gross, F. Ivars-Barcelo, A. Kotarba, S. Kondrat, B. Weckhuysen, B. Majumdar, A. Bruix, N. Fischer, B. Gates, J. Moulijn, A. Roldan, N. N. Tusar, T. Jakubek, D. Willock, M. Craven, K. Sethu, R. Catlow, R. Madix, H. Manyar, C. Friend, A. Corma, P. Wells, W. Ueda, A. Trunschke and R. Palmer, *Faraday Discuss.*, 2016, **188**, 131.
6 K. Moller and T. Bein, *Chem. Soc. Rev.*, 2013, **42**, 3689.
7 Y. Wei, T. E. Parmentier, K. P. de Jong and J. Zecevic, *Chem. Soc. Rev.*, 2015, **44**, 7234.
8 B. A. Holmberg, H. Wang and Y. Yan, *Microporous Mesoporous Mater.*, 2004, **74**, 189.
9 V. P. Valtchev, L. Tosheva and K. N. Bozhilov, *Langmuir*, 2005, **21**, 10724.
10 Z. Wan, W. Wu, W. Chen, H. Yang and D. Zhang, *Ind. Eng. Chem. Res.*, 2014, **53**, 19471.
11 S. van Donk, A. H. Janssen, J. H. Bitter and K. P. de Jong, *Catal. Rev.*, 2003, **45**, 297.
12 R. Zhang, P. Zhong, H. Arandiyan, Y. Guan, J. Liu, N. Wang, Y. Jiao and X. Fan, *Front. Chem. Sci. Eng.*, 2020, **14**, 275.
13 Y. Jiao, L. Forster, S. Xu, H. Chen, J. Han, X. Liu, Y. Zhou, J. Liu, J. Zhang, J. Yu, C. D'Agostino and X. Fan, *Angew. Chem., Int. Ed.*, 2020, DOI: 10.1002/anie.202002416.
14 X. Meng, F. Nawaz and F.-S. Xiao, *Nano Today*, 2009, **4**, 292.
15 J. Zhou, Z. Hua, J. Shi, Q. He, L. Guo and M. Ruan, *Chemistry*, 2009, **15**, 12949.
16 K. Möller and T. Bein, *Chem. Soc. Rev.*, 2013, **42**, 3689.
17 R. J. White, A. Fischer, C. Goebel and A. Thomas, *J. Am. Chem. Soc.*, 2014, **136**, 2715.
18 L. Wang, C. Yin, Z. Shan, S. Liu, Y. Du and F.-S. Xiao, *Colloids Surf., A*, 2009, **340**, 126.
19 A. Dufresne, *Mater. Today*, 2013, **16**, 220.
20 T. Abitbol, A. Rivkin, Y. Cao, Y. Nevo, E. Abraham, T. Ben-Shalom, S. Lapidot and O. Shoseyov, *Curr. Opin. Biotechnol.*, 2016, **39**, 76.
21 E. Dujardin, M. Blaseby and S. Mann, *J. Mater. Chem.*, 2003, **13**, 696.
22 K. E. Shopsowitz, H. Qi, W. Y. Hamad and M. J. MacLachlan, *Nature*, 2010, **468**, 422.
23 D. Shen, J. Liu, L. Gan, N. Huang and M. Long, *RSC Adv.*, 2017, **7**, 19237.
24 D. Shen, Y. Dai, J. Han, L. Gan, J. Liu and M. Long, *Chem. Eng. J.*, 2018, **332**, 563.
25 V. Valtchev, S. Mintova, I. Vulchev and V. Lazarova, *J. Chem. Soc., Chem. Commun.*, 1994, 2087.
26 S. Mintova and V. Valtchev, *Zeolites*, 1996, **16**, 31.
27 T. Sano, Y. Kiyozumi, K. Maeda, M. Toba, S.-i. Niwa and F. Mizukami, *J. Mater. Chem.*, 1992, **2**, 141.
28 B. Zhang, X. Li, Q. Wu, C. Zhang, Y. Yu, M. Lan, X. Wei, Z. Ying, T. Liu, G. Liang and F. Zhao, *Green Chem.*, 2016, **18**, 3315.
29 Y. Tao, H. Kanoh and K. Kaneko, *J. Phys. Chem. B*, 2003, **107**, 10974.
30 F. N. Gu, F. Wei, J. Y. Yang, N. Lin, W. G. Lin, Y. Wang and J. H. Zhu, *Chem. Mater.*, 2010, **22**, 2442.
31 W. Fu, L. Zhang, T. Tang, Q. Ke, S. Wang, J. Hu, G. Fang, J. Li and F.-S. Xiao, *J. Am. Chem. Soc.*, 2011, **133**, 15346.
32 S.-R. Zhai, W. Wei, D. Wu and Y.-H. Sun, *Catal. Lett.*, 2003, **89**, 261.
33 S. Zhai, Y. Zhang, D. Wu, Y. Sun and S. Wang, *Top. Catal.*, 2006, **39**, 227.
34 S.-R. Zhai, I. Kim and C.-S. Ha, *Catal. Today*, 2008, **131**, 55.
35 J. Qi, Q. Jin, K. Zhao and T. Zhao, *J. Porous Mater.*, 2015, **22**, 1021.
36 S. Candamano, P. Frontera, F. Crea and J. B. Nagya Rosario Aiello, in *Studies in Surface Science and Catalysis*, eds. A. Gédéon, P. Massiani and F. Babonneau, Elsevier, Amsterdam, 2008, vol. 174, pp. 237–240.
37 K. S. W. Sing and R. T. Williams, *Adsorpt. Sci. Technol.*, 2004, **22**, 773.
38 F. Delprato, J.-L. Guth, F. Hoffner and C. Zivkov, Synthesis of aluminosilicate zeolites of faujasite structure, *Fr. Pat*, 5192520, 1991.
39 L. Kunhao, V. Julia and G. M. Javier, *ChemCatChem*, 2014, **6**, 46.
40 J. García-Martínez, K. Li and G. Krishnaiah, *Chem. Commun.*, 2012, **48**, 11841.
41 S.-R. Zhai, W. Wei, D. Wu and Y.-H. Sun, *Catal. Lett.*, 2003, **89**, 261.
42 S.-R. Zhai, I. Kim and C.-S. Ha, *Catal. Today*, 2008, **131**, 55.
43 S. Al-Khattaf, J. A. Atias, K. Jarosch and H. de Lasa, *Chem. Eng. Sci.*, 2002, **57**, 4909.

44 J. A. Zhou, Z. L. Hua, Z. C. Liu, W. Wu, Y. Zhu and J. L. Shi, *ACS Catal.*, 2011, **1**, 287.
45 D. Yuan, C. Kang, W. Wang, H. Li, X. Zhu, Y. Wang, X. Gao, B. Wang, H. Zhao, C. Liu and B. Shen, *Catal. Sci. Technol.*, 2016, **6**, 8364.
46 J. G. Speight, *The Chemistry and technology of Petroleum*, CRC Press, Boca Raton, 4th edn, 2007.
47 J. Shi, Y. Wang, W. Yang, Y. Tang and Z. Xie, *Chem. Soc. Rev.*, 2015, **44**, 8877.